Journal of Biomolecular NMR, **22:** 333–347, 2002.
KLUWER/ESCOM

Solution structure determination of the two DNA-binding domains in the *Shizosaccharomyces pombe* Abp1 protein by a combination of dipolar coupling and diffusion anisotropy restraints

Jun Kikuchi[a], Junji Iwahara[b], Takanori Kigawa[a,b], Yota Murakami[c], Tsuneko Okazaki[d] & Shigeyuki Yokoyama[a,b,c]

[a]*RIKEN Genomic Sciences Center, Tsurumi, Yokohama 230-0045, Japan;* [b]*Cellular Signaling Laboratory, RIKEN Harima Institute at SPring-8, Sayo-gun, Hyogo 679-5148, Japan;* [c]*Department of Viral Oncology, Institute for Virus Research, Kyoto University, Sakyo-ku, Kyoto 606, Japan;* [d]*Institute for Comprehensive Medical Science, Fujita Health University, Toyoake, Aichi 470-11, Japan;* [e]*Department of Biophysics and Biochemistry, Graduate School of Science, The University of Tokyo, Bunkyo-ku, Tokyo 113-0033, Japan*

Received 26 October 2001; Accepted 16 January 2002

Key words: alignment tensor, domain orientation, residual dipolar coupling, rotational diffusion anisotropy

Abstract

We have solved the solution structure of the N-terminal region of the fission yeast centromere protein, Abp1, bound to a 21-base pair DNA fragment bearing its recognition site (Mw = 30 kDa). Although the two DNA-binding domains in the Abp1 protein were defined well by a conventional NOE-based NMR methodology, the overall structure of the Abp1 protein was poorly defined, due to the lack of interdomain distance restraints. Therefore, we additionally used residual dipolar couplings measured in a weakly aligned state, and rotational diffusion anisotropies. Neither the NH residual dipolar couplings nor the backbone ^{15}N T_1/T_2 data were sufficient to determine the overall structure of the Abp1 protein, due to spectral overlap. We used a combination of these two orientational restraints (residual dipolar coupling and rotational diffusion anisotropy), which significantly improved the convergence of the overall structures. The range of the observed T_1/T_2 ratios was wider (20–50 for the secondary structure regions of Abp1) than the previously reported data for several globular proteins, indicating that the overall shape of the Abp1•DNA complex is ellipsoid. This extended form would facilitate the recognition of the two separate sites in the relatively long DNA sequence by the DNA-binding domains of Apb1.

Introduction

During the last five years, novel approaches toward obtaining orientational information relative to a common molecular reference frame have been proposed as new tools for the structure determinations of proteins and nucleic acids. These parameters are heteronuclear relaxation in anisotropically tumbling molecules (Brüschweiler et al., 1995; Tjandra et al., 1995) and residual dipolar couplings (Tolman et al., 1995; King et al. 1995). Heteronuclear relaxation analysis has now been established as an important tool for the investigation of molecular dynamics by NMR spectroscopy (Kay et al., 1989). Recently, these data were used to study the hydrodynamic properties of proteins (Barbato et al., 1992; Brüschweiler et al., 1995; Tjandra et al., 1995). Due to the orientational dependency of the heteronuclear relaxation data (T_1/T_2) with respect to the diffusion axis of a protein, they are useful to characterize the relative orientation of two domains (Fushman et al., 1999; Smith et al., 2000; Campos-Olivas et al., 2000). Furthermore, Tjandra et al. showed that the dependence of heteronuclear relaxation times on rotational diffusion anisotropy can provide orientational restraints for a simulated annealing structure (Tjandra et al., 1997a). This approach has

*To whom correspondence should be addressed. E-mail: yokoyama@biochem.s.u-tokyo.ac.jp

been extended to the structure determinations of cytochrome c′ (Tsan et al., 2000) and ribosome recycling factor (Yoshida et al., 2001). Furthermore, the solution structure of a fibronectin module pair, which has a tiny connection between the two domains, has also been determined using T_1/T_2 restraints with a small number of interdomain NOEs (Hashimoto et al., 2000).

The weak alignment of protein molecules in solution, which is induced either by the magnetic-field (Tolman et al., 1995), or by liquid crystalline media (Tjandra and Bax, 1997), prevents the complete averaging of the dipolar interactions, which would provide information on the orientations of internuclear vectors. By incorporating the orientational data in simulated annealing protocols for structure determinations, more than twenty protein structures have already been solved with higher precision. In particular, residual dipolar couplings provide long-range order restraints which, in combination with classical NOE data, successfully improve the domain orientations in multi-domain systems, such as ribosomal protein S4 (Markus et al., 1999), barley lectin (Fischer et al., 1999), zinc finger (Tsui et al., 2000), and T4 lysozyme (Goto et al., 2001).

The *Shizosaccharomyces pombe* Abp1 protein is localized in the centromere of the chromosome, and has two DNA-binding domains in its N-terminal region (Murakami et al., 1996). In the present study, we tried to determine the solution structure of the Abp1 N-terminal-region fragment (designated as 'the Abp1 protein' or 'Abp1' hereafter in this paper) in a complex with a specific 21 base pair DNA fragment. We had several problems with the spectral analysis and the structure calculation of the Abp1 protein. First, we could determine the domain structures but had a poor convergence of the overall structure, probably because we lacked NOE data for the contact between the two DNA-binding domains. Second, the ^{1}H-^{15}N HSQC spectrum exhibited significant spectral overlap due to the high helical content and the relatively large molecular size (30 kDa). Therefore, neither the residual dipolar coupling data nor the rotational diffusion data contributed largely to the overall structure convergence. Nevertheless, the rotational diffusion data that could be obtained appeared to be effective, probably because of the elongated shape of the Abp1•DNA complex. Therefore, we used both the rotational diffusion anisotropy and the residual dipolar coupling restraints, and succeeded in the overall structure determination of the Abp1 protein in the DNA-bound state.

Methods

NMR spectroscopy

All NMR experiments were carried out at pH 6.8 and 310 K on 1 mM solutions containing a 1:1 molar ratio of the *Shizosaccharomyces pombe* Abp1 protein and a double stranded 21 bp oligonucleotide. The N-terminal DNA-binding region of Abp1 was uniformly labeled with ^{15}N or ^{15}N/^{13}C. Detailed information for the purification of the Abp1 protein and its complex formation will be published elsewhere (J. Kikuchi et al., in preparation). Random 60% ^{2}H labeling was performed on Abp1 to reduce the loss of magnetization transfer due to its relatively large molecular weight in the complex (see the following section). The ^{1}H, ^{13}C and ^{15}N sequential assignments were obtained using 3D double and triple resonance through-bond correlation experiments, such as HNCO, HN(CA)CO, HNCA, HN(CO)CA, CBCA(CO)NH, CBCANH, HBHA(CBCACO)NH, H(CCO)NH, HCCH-COSY, and HCCH-TOCSY, with occasional deuterium decouplings. The details of most experiments, together with the original references, are provided in reviews (Bax and Grzesiek, 1993). The mixing times of the NOE experiments for the 2D ^{1}H-^{1}H, 3D ^{13}C-separated, and 3D ^{15}N-separated spectra varied from 80 ms to 180 ms. All through-bond type and through-space type NMR experiments were performed using a Bruker DRX-600 NMR spectrometer.

The residual dipolar couplings were measured in two ways: either by the measurement of the magnetic field-dependent $^1J_{NH}$ changes, or by the difference between the anisotropic and isotropic phases. In the former case, the magnetic field strengths employed were 400, 500, 600, and 800 MHz (^{1}H frequency). In the latter case, we used two kinds of media as the anisotropic phase. The liquid crystal sample contained 5.0 wt % bicelle (molar ratio of [DMPC]/[DHPC] = 3.0), 0.3 mM Abp1•DNA, 0.1% NaN_3, and 5% ^2H_2O. The other anisotropic medium we employed was a nematic liquid crystalline state of a Pf1 phage solution (Hansen et al., 1998). The finally optimized Pf1 phage concentration was 12 mg/mL for 0.3 mM Abp1•DNA (see the following section). The 2D IPAP [^{1}H-^{15}N] experiment was used to measure the $^1J_{NH}$ values (Ottiger et al., 1998). A total of 512 complex f1 (^{15}N) and 4096 complex f2 (^{1}H) points were recorded with 24 scans per f1 increment for the isotropic sample. A total of 96 scans per f1 increment were recorded for both of the anisotropic

samples. Spectral widths were 1399 Hz and 15576 Hz for f1 and f2, respectively. The indirect dimension was zero-filled to 2048 points in the final data matrix. A Gaussian apodization window was used to process the f1 and f2 free induction decays.

The ^{1}H-^{15}N heteronuclear NOE (hNOE) measurements were performed according to the method described in Grzesiek and Bax (1993). ^{15}N spin-lock pulses spaced 1.2 ms apart were used in the T_2 experiments to minimize the resonance offset effects and the lack of field homogeneity. For T_1 measurements, eight delays of 12, 36, 76, 124, 324, 444, 804 and 1604 ms, and for T_2 measurements, eight delays of 2.5, 7.5, 12.5, 17.5, 22.5, 32.5, 47.5, 97.5 ms, were used. For both T_1 and T_2 measurements, a recycle delay of 3.0 seconds was used. Processing of relaxation spectra was done by applying a Lorentzian-to-Gaussian transformation with a Lorentzian linewidth of 15 Hz and a Gaussian linewidth of 20 Hz in both dimensions, in order to quantify the signal intensities (Mandel et al., 1995).

Analysis of rotational diffusion anisotropy

The values of the ^{15}N relaxation times were analyzed by assuming dipolar and CSA relaxation with 1.02 Å for the NH bond length and -170 ppm for the chemical shift anisotropy of (Tjandra et al., 1996). The analysis of the overall tumbling of Abp1•DNA from the T_1/T_2 data of backbone amide groups was carried out with the program TENSOR (Dosset et al., 2000). Three models were tested: a sphere ($D_{zz} = D_{yy} = D_{xx}$, $D_{\rm iso} = (D_{zz} + D_{yy} + D_{xx})/3$), an axially symmetric tensor ($D_{zz} \neq D_{yy} = D_{xx}$, $D_{\parallel} = D_{zz}$ and $D_{\perp} = (D_{xx} + D_{yy})/2$), and a fully asymmetric tensor ($D_{zz} \neq D_{yy} \neq D_{xx}$) (Woessner, 1962). The inertial tensor parameters ($\{D_{\rm iso}\}$, $\{D_{\parallel}, D_{\perp}, \phi, \psi\}$, and $\{D_{zz}, D_{yy}, D_{xx}, \phi, \psi, \theta\}$) for the isotropic, axially symmetric, and fully asymmetric models were fitted to the experimental data via χ^2 minimization (Tsan et al., 2000). The local diffusion constant can be related to the local diffusion correlation time. The fitting of the diffusion tensor components and the orientation was performed using a simulated annealing algorithm written in the TENSOR program.

Hydrodynamic calculation

Hydrodynamic calculations were performed using the program HYDRONMR (García de la Torre et al., 2000). This program can calculate the hydrodynamic properties of proteins without using bead models of the NMR structures prior to input, whereas the previous versions of their programs, HYDRO or SOLPRO required definition of the bead models. The temperature was set to 310 K, the viscosity was taken as 7.0×10^{-4} Nsm^{-2}, and the atomic element radius (AER) was set to 3.1 Å.

Structure calculations

The NOE-derived interproton distance restraints were classified into four categories: 1.8–2.7 Å, 1.8–3.5 Å, 1.8–5.0 Å, and 1.8–6.0 Å, corresponding to strong, medium, weak, and very weak NOEs, respectively. The hydrogen bond restraints (two per hydrogen bond) were rNH-O = 1.7–2.5 Å and rN-O = 2.7–3.3 Å, which were obtained from the NH chemical shift temperature coefficients (δHN/δT < -2 ppb/K) (Anderson et al., 1997), and the backbone NOE patterns. The backbone ϕ, ψ torsion angles were restrained by the conformational dependency of the Cα and Cβ chemical shifts as well as the following residue type dependency in the C$'$ chemical shifts, using the program TALOS (Cornilescu et al., 1998). The residual dipolar coupling based restraints as well as the rotational diffusion anisotropy restraints have been used in the SANI and DANI modules (Clore et al., 1998a) for performing direct refinement against the measured dipolar couplings and the rotational diffusion anisotropies by the program CNS version 1.0 (Brünger et al., 1998). Structure calculations were performed starting from extended structures (Nilges et al., 1988) in torsion angle space dynamics (TAD) followed by Cartesian minimization (Stein et al., 1997). An initial TAD (hot) phase was performed at a temperature of 50 000 K and consisted of 10 000 molecular dynamics steps of 15 fs each. Subsequently, a TAD cooling phase comprising of 60 000 steps of 2 fs each was employed, with temperature annealing from 50 000 K to 0 K during this stage. All parameters were scaled to default values. A second cooling stage in TAD was employed for 40 000 steps of 1 ps each, with temperature annealing from 1000 K to 0 K. The final values for the force constants employed for the energy minimization step were as follows: 1000 kcal mol^{-1} Å^{-2} for bond lengths, 500 kcal mol^{-1} rad^{-2} for angles and improper torsions (which maintain planarity and chirality), 4 kcal mol^{-1} Å^{-2} for the quadratic van der Waals repulsion term, 50 kcal mol^{-1} Å^{-4} for experimental distance restraints, 1.0 kcal mol^{-1} Hz^{-2} for $^{1}D_{\rm NH}$ residual dipolar coupling restraints, and 0.5 kcal mol^{-1} for diffusion anisotropy restraints.

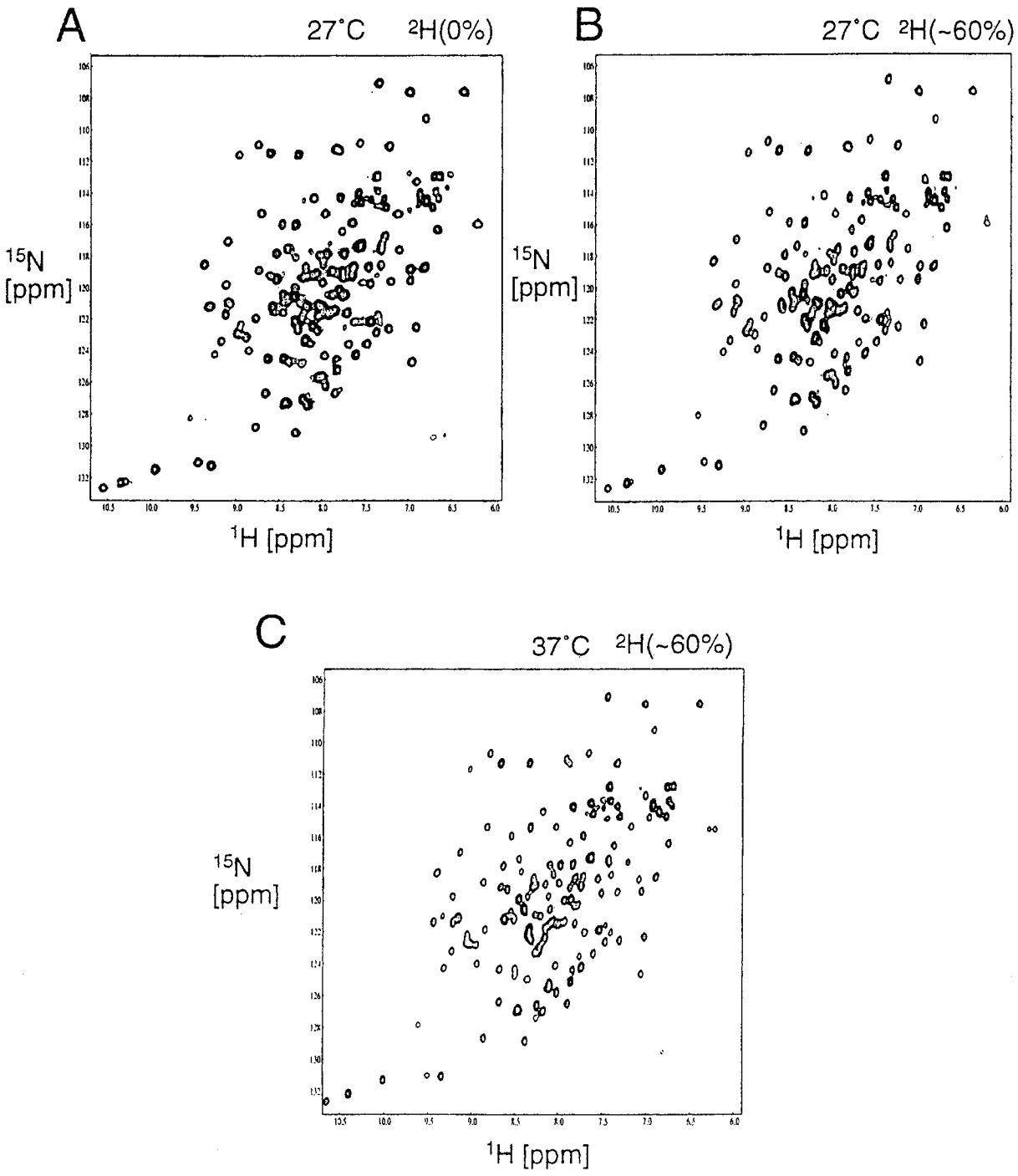

Figure 1. Comparison of the ^{1}H-^{15}N HSQC spectra of the protonated and 60%-deuterated ^{15}N-labeled Abp1•DNA complex observed at 600 MHz ^{1}H frequency. (A) Protonated Abp1•DNA at 300 K. (B) 60%-deuterated Abp1•DNA at 300 K. (C) 60%-deuterated Abp1•DNA at 310K.

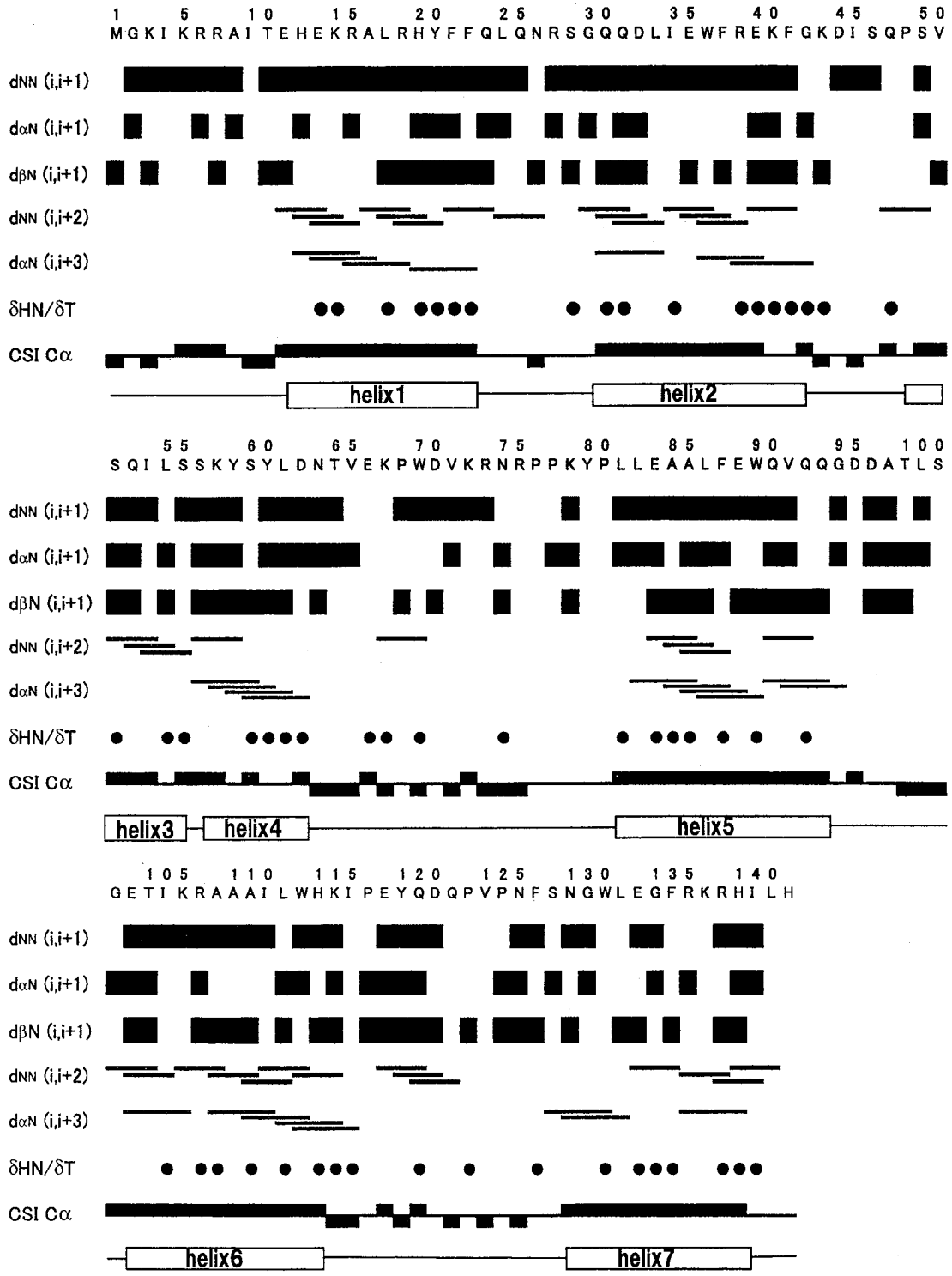

Figure 2. Summary of the observed sequential NOEs, the temperature dependence of the amide proton chemical shifts (δHN/dT), and the chemical shift index (CSI) of Cα, together with the derived secondary structure of Abp1 whilst complexed to DNA.

Results and discussion

Spectral analysis of the NMR conditions for the Abp1•DNA complex

The Abp1•DNA complex presented a difficult problem for spectral analysis by NMR. First, the chemical shift dispersion was limited, on account of the large amount of helix in the structure (see the following text). Secondly, the line widths were relatively large, due to its high molecular weight (approximately 30 kDa) and elliptical molecular shape (see below). The line width can be narrowed by deuteration of the protein. Thus, the average T_2 for the backbone amide nitrogens increased by about 1.5- fold, from roughly 25 ms for $^{1}H/^{15}N$-labeled Abp1•DNA to 40 ms for $^{2}H/^{15}N$ Abp1•DNA. These T_2 values were slightly larger than those for the N-terminal domain of Enzyme I, which has a similar molecular weight (Garrett et al., 1997). The N-terminal region of Abp1 consists of 141 residues, including 5 proline residues, for which a total of 135 ^{1}H-^{15}N cross-peaks arising from all backbone amide resonances, except for the N-terminal amino group, were expected in the ^{1}H-^{15}N HSQC spectra. Due to its relatively large molecular size (30 kDa), the ^{1}H-^{15}N cross-peaks were broadened in the HSQC spectrum, even at a high temperature. Since the Abp1 protein is not expressed well in *E. coli*, nearly 100% deuteration would be time- and cost-prohibitive. Therefore, we chose 60% random deuteration of the Abp1 protein for T_2 optimization. In the fractionally deuterated sample, we observed several HSQC spectra at different temperatures from 290 K to 325 K, and found that the significant overlaps were slightly improved at 310 K (Figure 1C). The backbone sequential assignments were made by using sensitive triple resonance experiments, such as HNCO, HNCA, HN(CO)CA and HN(CA)CO, with deuterium decoupling. Widely used triple resonance spectra, such as CBCANH and CBCA(CO)NH spectra with deuterium decoupling, were used to confirm the assigned resonances, although the signal qualities were poor. The reduction in the cross peak intensities was significant in the case of the side-chain through-bond type experiments, such as HCCH-COSY, HCCH-TOCSY and HC(CCO)NH. By the combined use of these through-bond type experiments and the 3D ^{15}N-edited or ^{13}C-edited NOESY-HSQC spectra, the protein side-chain assignments were accomplished. The assignments of the long side-chain residues, such as Lys and Arg, were difficult, because of the low incorporation of deuterium from $^{2}H_2O$ in long biosynthetic pathways (Gardner and Kay, 1998), and therefore, the dipolar relaxation of the CH groups was still severe.

Low precision of the overall Abp1 structure calculated from NOE-based distance restraints and TALOS-derived dihedral angle restraints

The experimental secondary structure identification was achieved using a combination of the chemical shift index method and the characteristic NOE patterns. Figure 2 shows a summary of the secondary shift patterns and the NOE patterns against the Abp1 residue number. The observation of the characteristic NOE pattern $d_{\alpha_N}\, i, i+3$ was sometimes difficult, due to the low proton density. However, CSI was useful to identify the helical region.

The solution structure of the Abp1 protein complexed with the 21-bp DNA was calculated by a simulated annealing protocol using the restrained molecular dynamics program, CNS. Interproton distance restraints were derived from 3D ^{15}N-edited, 3D ^{13}C-edited NOESY-HSQC and 4D ^{13}C, ^{15}N-edited NOESY-HSQC spectra. Initially, the structure calculations were performed using only these NOE-based distance restraints. The subsequent addition of hydrogen bond restraints neither increased the total energy nor violated the distance restraints set.

A total of 117 ϕ and ψ dihedral angle restraints were included in the next structure calculation. The solution structure of the Abp1 protein is composed of two structurally independent domains, which are both folded in a helix-turn-helix motif. Here we defined a domain boundary in the center of the domain linkers: Domain 1 comprises residues M1 to K72 and domain 2 comprises residues R73 to H141. Ensembles of the overall structures, aligned on the core backbone coordinates of each of the two domains, are shown in Figures 3A and 3B). The Abp1 protein comprises seven helices with two well-defined loop regions near the N-terminus (residues K3 to T10) and an interdomain linker (residues T64 to P80). These loops exhibit relatively rigid relaxation parameters, especially in the T_2 and hNOE data. In spite of the restricted backbone motion in the interdomain linker region, the number of NOEs observed here was much smaller than elsewhere in the structure. Therefore, the interdomain orientation was poorly defined (Figure 3C). The root-mean-squared differences (R.M.S.D.) of the backbone nuclei of domains 1 and 2 were 1.07±0.17 Å and 0.83±0.25 Å, respectively (Table 1). In contrast to

the well-converged structure of each domain, the overall structure of Abp1 was poorly defined (backbone R.M.S.D. = 9.13±2.30 Å).

Choice of anisotropic media for measurements of residual dipolar couplings

The $^1D_{NH}$ dipolar coupling restraints were utilized in addition to the distance and dihedral angle restraints derived from standard heteronuclear NMR experiments. The dipolar coupling between two nuclei yields the orientation of the internuclear bond vector relative to the overall molecular alignment tensor. Residual dipolar couplings can be measured at a high magnetic field for macromolecules with non-zero anisotropic magnetic susceptibility. Early observations of the residual dipolar couplings in biomacromolecules have used this effect to obtain a residual dipolar coupling on the order of ± 2 Hz (King et al., 1995; Tolman et al., 1995). This was applied to the GATA-1/DNA complex to produce orientational restraints in the NMR structure calculation (Tjandra et al., 1997b). We tried this method to obtain the NH residual dipolar couplings, using magnetic field strengths ranging from 9.4 T to 18.8 T. Due to the high magnetic susceptibility arising from the abundant aromatic system of the DNA (21 bp), the observed NH residual dipolar couplings were twice those seen previously for GATA-1/DNA. We incorporated these $^1D_{\mathrm{NH}}$ values into the CNS structure calculation of the Abp1 protein. However, these orientational restraints were not useful to determine the overall structure of the Abp1. The main problem was the quantitative uncertainty in the restraints, due to the spectral overlap at the low magnetic field. Recently, it was shown that dissolving macromolecules in a dilute liquid crystal phase produces a larger and adjustable degree of alignment (Tjandra and Bax, 1997). The liquid crystal used was a disk- shaped phospholipid bilayer called a bicelle, which can be aligned in the magnetic field. Therefore, as a second trial, we introduced an alignment using the liquid crystalline bicelle. In the case of the directly bonded nuclei, the dipolar couplings are distance-constant and contain orientational information. From the quadrupolar splittings of the HO^{2}H signal and the chemical shift anisotropy (CSA)-induced chemical shift changes in the ^{31}P-NMR spectra, we confirmed the alignment of the bicelle between 300 K and 315 K. However, significant aggregation occurred when the Abp1•DNA complex was mixed in the bicelle media. This phenomenon may have resulted from an electrostatic interaction between the lipids and the positively-charged surface of Abp1. Finally, we chose a Pf1 phage solution as a nematic phase, liquid crystalline medium to obtain a weakly aligned state of the protein (Hansen et al., 1998). The magnitudes of the quadrupolar splittings of the HO^{2}H signals increased as a function of the Pf1 phage concentration (data not shown). However, the [^{1}H-^{15}N] cross peaks in the IPAP-HSQC spectra were broadened by an excess amount of Pf1 phage. The signal quality did not change with the addition of NaCl, which may suppress the electrostatic interactions between the phage and the protein (Markus et al., 1999). The addition of NaCl may weaken the electrostatic interaction between the Abp1•DNA complex and the Pf1 phage, and simultaneously reduce the Abp1•DNA interaction. In our experience, 0.3 mM Abp1•DNA with 12 mg/ml of Pf1 phage was the best condition to observe the NH residual dipolar couplings.

Difficulties in analyzing the residual dipolar coupling data

The experimental NH residual dipolar couplings ($^1D_{\mathrm{NH}}$) were obtained from the difference between the anisotropic (with phage) and the isotropic (without phage) $^1J_{\mathrm{NH}}$ values. Due to the high helical content of Abp1, the chemical shift dispersion was poor, as seen in Figure 1. In addition to this, the relatively low concentration of the Abp1•DNA complex in the phage medium and the broadened signals thwarted our attempts to obtain a better quality [^{1}H-^{15}N] IPAP-HSQC spectrum. After excluding the residues exhibiting [^{1}H-^{15}N] NOE < 0.6 and overlapped signals, we chose only 47 residues of the $^1D_{\mathrm{NH}}$ data (35% of the total of 141 residues, excluding 5 prolines) as the orientational restraints. The magnitude of the observed dipolar couplings was on the order of ± 25 Hz. Initial estimations of the magnitude of the axial (−12.5 Hz) and rhombic (0.4) components of the alignment tensors were obtained by examining the powder pattern distribution of the dipolar couplings (Clore et al., 1998b). Incorporation of the NH residual dipolar coupling restraints did not induce any significant structural change in either DNA-binding domain (Table 1 [II]). In spite of the improved convergence (RMSD = ca. 2 Å), it was still difficult to elucidate the relative positions of the two recognition helices in each domain (Figure 3D).

Table 1. Structural statistics of the solution structures of Abp1, with and without the use of T_1/T_2 and $^1D_{NH}$ orientational restraints

R.M.S.D. from experimental restraints for final structures				
Distances (Å)	0.021 ± 0.003			
Dihedrals (deg)	1.43 ± 0.81			
T_1/T_2 ratios	1.17 ± 0.32			
$^1D_{NH}$ (Hz)	1.17 ± 0.33			
R.M.S.D. from idealized covalent geometry				
Bonds (Å)	0.002 ± 0.003			
Angles (deg)	0.54 ± 0.07			
Impropers (deg)	0.32 ± 0.05			
	[I] (distance and angle only)	[II] ([I] + $^1D_{NH}$)	[III] ([I] + T_1/T_2)	[IV] ([III] + T_1/T_2)
Precision of the selected ensemble structures represented as RMSD values (Å)[a]				
(a) Backbone	1.07 ± 0.17	1.36 ± 0.36	0.82 ± 0.14	0.85 ± 0.20
All heavy	2.12 ± 0.21	2.15 ± 0.34	1.96 ± 0.21	1.70 ± 0.24
(b) Backbone	0.83 ± 0.25	1.34 ± 0.28	1.01 ± 0.24	1.20 ± 0.28
All heavy	1.74 ± 0.26	2.22 ± 0.35	1.92 ± 0.20	1.99 ± 0.26
(c) Backbone	9.13 ± 2.30	6.96 ± 3.54	4.21 ± 0.88	1.95 ± 0.44
All heavy	9.69 ± 2.37	7.46 ± 3.50	4.96 ± 0.82	2.53 ± 0.37
Number of restraints used in the CNS calculation				
Distances	1889	1889	1889	1889
TALOS-derived angle	117	117	117	117
$^1D_{NH}$ in Pf1 phage	–	47	–	47
T_1/T_2 in solution	–	–	52	48

[a]These RMSD values were calculated for the ensemble solution structures superimposed on the helical regions of (a) domain 1 (E11-Q23, G29-G43, S49-S55, S56-N64), (b) domain 2 (L81-Q93, E102-I115, W130-I139), and (c) domains 1 and 2.

A common rotational diffusion tensor was assumed for the two DNA-binding domains in the Abp1•DNA complex

Ramirez and Bax (1998) pointed out that the introduction of two different orientational tensors allowed the orientations of the N-H bond vectors to be defined by the intersection of two taco-shaped rings, which is far more restrictive than either one alone. As we have described, however, the trials of the other alignment methods failed, due to the problem of this sample-specific characteristic. Yoshida et al. (2001) reported that the ribosome recycling factor, with a highly anisotropic molecular shape exhibits a wide distribution of T_1/T_2 ratios, also found with the enzyme-1 (Tjandra et al., 1997a). In the present study, the Abp1 protein consists of the two DNA-binding domains, and is bound with a relatively long DNA fragment. Therefore, we may expect a significantly wide distribution of the T_1/T_2 ratios, reflecting the elongated molecular shape. Thus, we decided to use the rotational diffusion anisotropy data as the second orientational restraints. The Abp1-bound DNA seems to be rigid, because the line widths of all of the imino protons, except for those of the 5′- and 3′-terminal residues, were narrow (data not shown). Actually, the sequential assignment of the observable imino proton resonances was successful with the NOESY spectra. There was no sign of slow or intermediate chemical exchange in the NMR spectra of the Abp1•DNA complex. Therefore, it is likely that the relative motions of the two domains are restricted in the DNA-bound state. Thus, a common rotational diffusion tensor may be assumed for the two DNA-binding domains in the Abp1•DNA complex.

Relaxation analysis of the Abp1•DNA complex indicates significant anisotropic diffusion in solution

The motional dynamics of the Abp1•DNA complex were investigated by determining the nuclear relax-

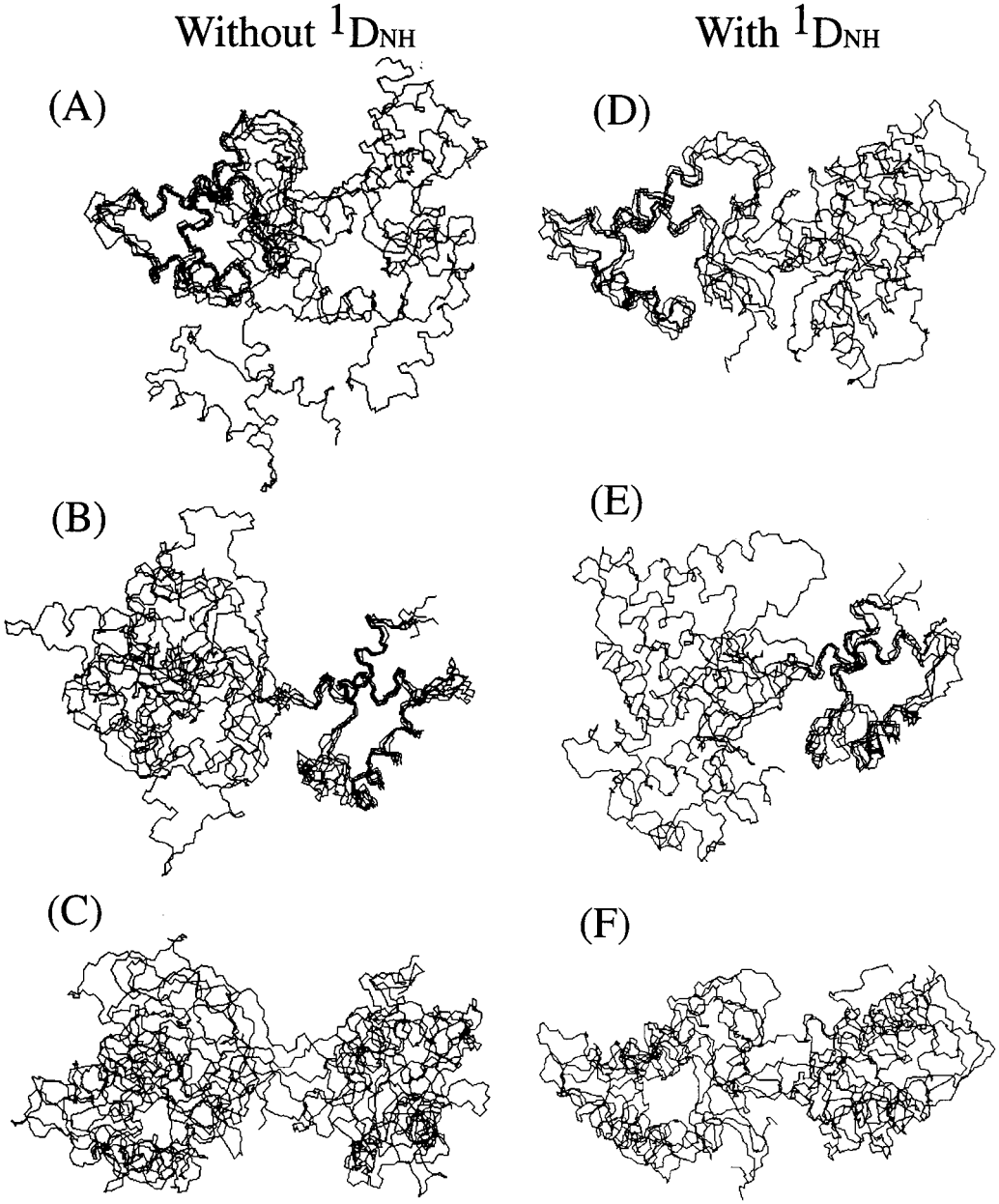

Figure 3. Comparison of the selected ensemble of structures calculated without (left) and with (right) NH residual dipolar couplings in the CNS calculation of Abp1, superimposed with domain 1 (A), (D); domain 2 (B), (E); and domains 1 and 2 (C), (F). Residues used for superimposition are: E11-Q23, G29-G43, S49-S55, and S56-N64 for domain 1, and L81-Q93, E102-I115, and W130-I139 for domain 2.

ation properties of the backbone amide groups in the protein. The parameters included the [^{1}H-^{15}N] heteronuclear NOE enhancement (hNOE), the ^{15}N longitudinal relaxation rates T_1, and the ^{15}N transverse relaxation rates T_2 (Figure 4). Due to the rapid solvent-exchange rates exhibited by the backbone amide groups in the Abp1•DNA complex, gradient-based pulse sequences were used to minimize the effects of solvent exchange. The average T_2 values in the helical regions were 35 ms, and the average hNOE values were 0.8. In addition to the helical regions, the long loop regions, such as the N-terminus (K3 to T10) and the interdomain linker, behave as structured regions according to these relaxation data.

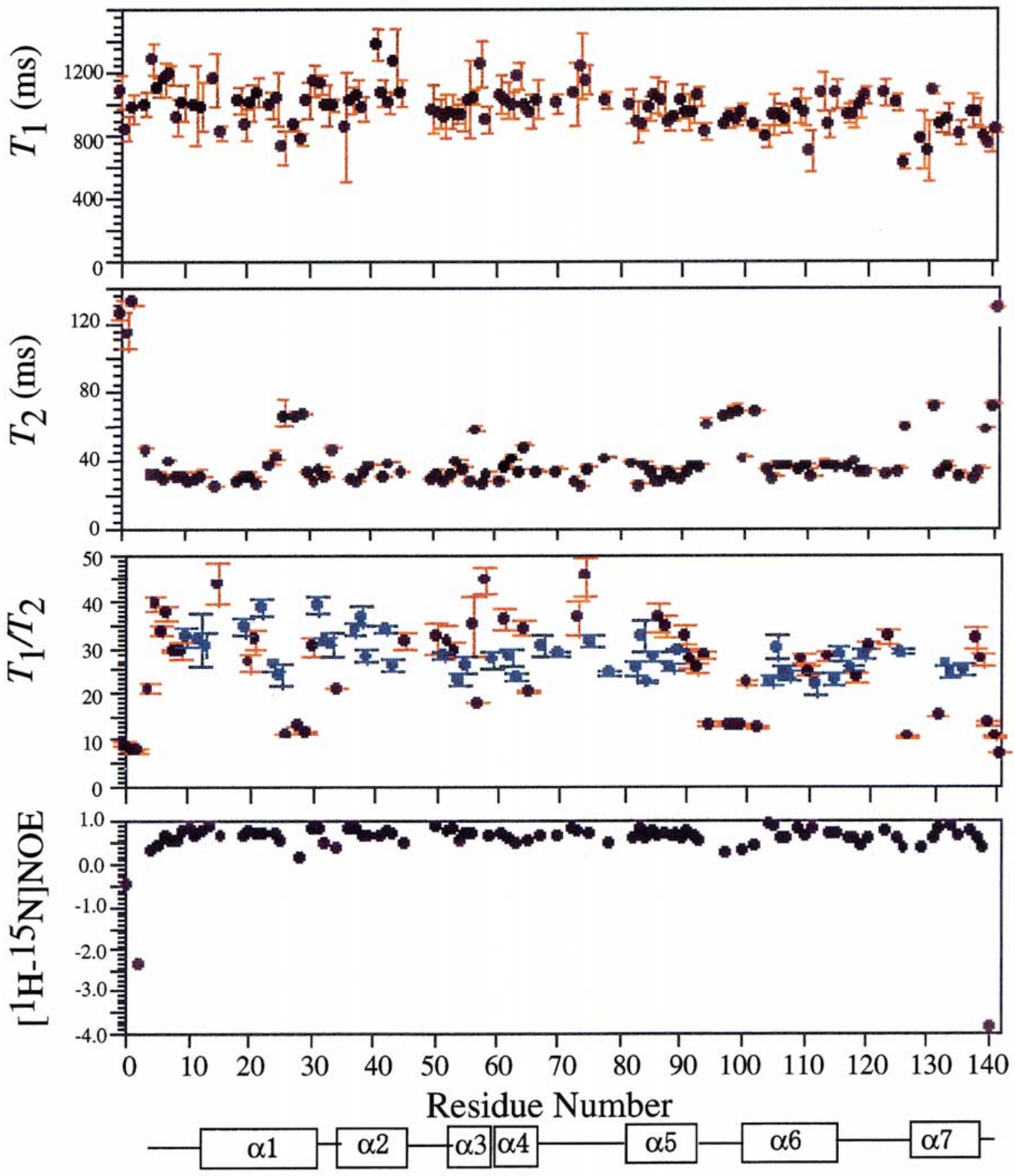

Figure 4. Backbone ^{15}N relaxation parameters for individual residues of the Abp1•DNA complex at a 600MHz ^{1}H frequency. (A) T_1 (ms), (B) T_2 (ms), (C) (T_1/T_2), and (D) ^{1}H-^{15}N NOE. The locations of the helices are indicated below. Gaps correspond to prolines, or to residues with values that could not be measured because of spectral overlap. The T_1/T_2 data used in the final state of the CNS structure calculation are colored with blue, respectively.

This is a consequence of DNA binding, as discussed in the following section.

Similar results were reported for the complexes of several other DNA-binding proteins, which exhibit anisotropic diffusion due to their ellipsoid molecular shapes. The T_1/T_2 ratio is useful for estimating the effective correlation time of the molecular rotational diffusion in the nanosecond range, and is roughly independent of the order parameter and the fast internal motions with a small amplitude. In addition to this, Tjandra et al. (1997a) pointed out that the individual T_1/T_2ratios provide a direct measure of the angle between the N-H bond vector and the unique axis of the diffusion tensor. The T_1/T_2 ratios of the Abp1•DNA complex had a significantly wider distribution than those previously reported (Figure 4).

Overall rotational diffusion constants and anisotropy

Time constants for rotational diffusion were calculated, based on the T_1/T_2 data. For the amide groups with restricted local dynamics, the local internuclear vector orientations can be derived from the observed T_1/T_2 ratio values. We need initial estimations of the overall correlation time, and the axial and rhombic components in the structure calculations of proteins (Tjandra et al., 1997a). The apparent correlation time, τ_{app}, can be determined from the individual T_1/T_2 data for the NH groups in advance of the structure calculation, using $\tau_{app} = (2\omega_N)^{-1}\ (6T_1/T_2\text{-}7)^{1/2}$ (Fushman et al., 1994). In the case of isotropic rotational diffusion (with $D_{||} = D_\perp$), τ_{app} coincides with the overall (isotropic) correlation time, τ_c. The observed τ_{app} value of 14 ns is reasonably similar to that of a 30-kDa protein, as compared to the previously reported globular proteins.

After excluding the insufficiently resolved ^{1}H-^{15}N correlation peaks, as well as the amides that undergo significant internal motions faster than the overall rotational diffusion rate (characterized by ^{1}H-^{15}N NOE < 0.6), 67 T_1/T_2 data were available for analysis: 59 from the helical regions and 7 from the loop regions. Although many of the T_1/T_2 data are not flat within helical regions, this would be reflected as curvature or non-ideal geometry of these helices. Even assuming ideal helical geometry, however, the predicted T_1/T_2 data have a periodic pattern (data not shown).

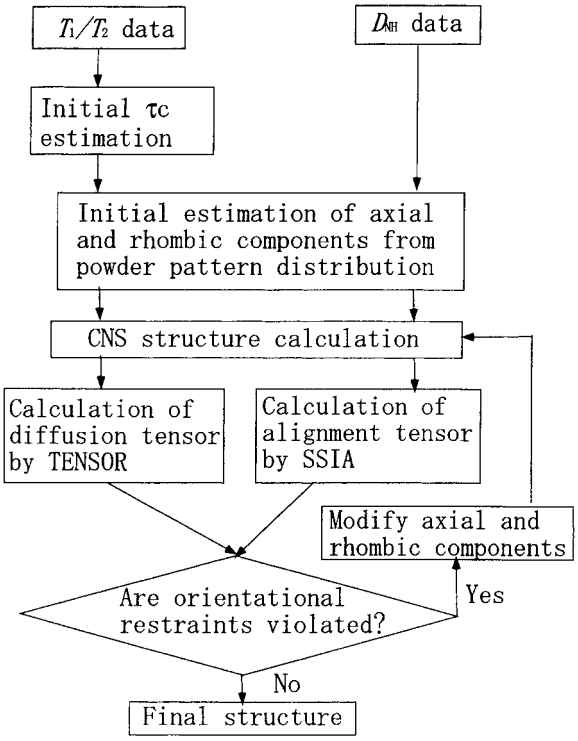

Figure 5. Flow chart showing how the residual dipolar coupling and the rotational diffusion anisotropy restraints are incorporated into the structure calculation scheme.

The combination of rotational diffusion anisotropy restraints and dipolar coupling restraints significantly improves the domain orientation definition

As anticipated, the use of the T_1/T_2 ratios instead of the residual dipolar coupling data did not considerably improve the convergence of the overall structure of Abp1 (Table 1). Therefore, we used both the T_1/T_2 ratios and the residual dipolar coupling data as constraints in the structure calculation. Figure 5 shows the optimization of the diffusion and alignment parameters during the structure calculation step. The ^{15}N T_1/T_2 ratios of Abp1•DNA were fit to the lowest energy structure calculated with the dipolar couplings, with an initial estimation of the alignment parameters using the powder pattern distribution of the $^1D_{NH}$ data. The powder pattern of the residual dipolar coupling data differs from the lowest extreme value (A_{yy}) and the most populated value (A_{xx}). Therefore, the alignment tensor is not axially symmetric. The diffusion parameters were derived from the program TENSOR (Dosset et al., 2000), and the alignment parameters were re-evaluated using the program SSIA (Zweckstetter and Bax, 2000). The structure calcula-

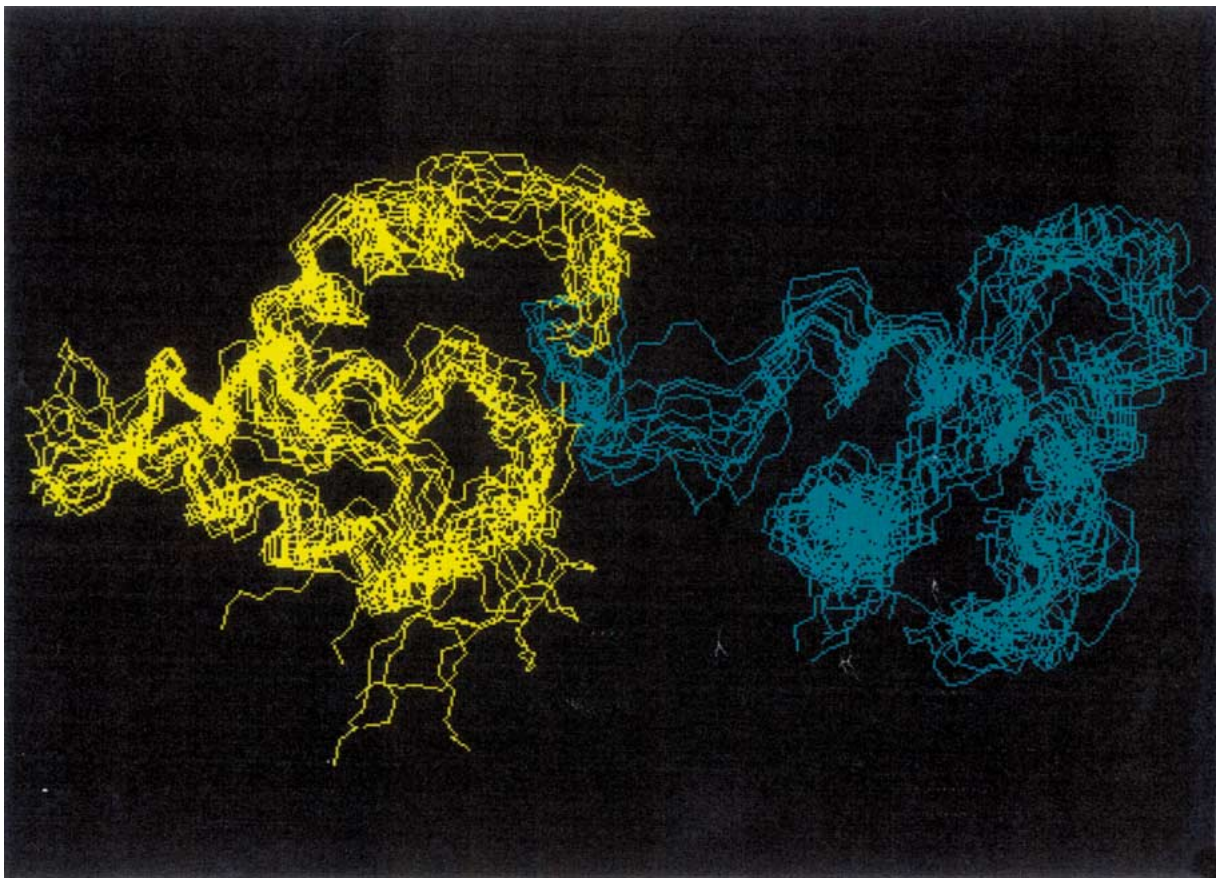

Figure 6. Superimposition of the 10-converged structures of Abp1 derived from NOE, hydrogen bond, TALOS-based dihedral angle, T_1/T_2 rotational diffusion, and NH residual dipolar coupling restraints. Domain 1 is shown in yellow and domain 2 is in cyan. The relative orientation of the two DNA-binding regions was significantly restricted by the introduction of both the residual dipolar couplings and the rotational diffusion anisotropy restraints.

tion without using the residual dipolar coupling data (case [III] in Table 1) did not improve the precision of the overall structures, respectively. We repeated the refinements of these parameters using the lowest energy structures in each step, as shown in Figure 5. Firstly, we checked violation of both the residual dipolar coupling restraints and the rotational diffusion restraints. We deleted the restraints that exhibit significant violations in the ensemble of the structures. Furthermore, axial and rhombic components were evaluated using the program SSIA and TENSOR. We repeated 101 times of the CNS structure calculations and these evaluations. The final fitted axial factor of the diffusion anisotropy (defined as $D_{||}/D_{\perp}$) is 2.1, with an effective correlation time of 14.2 ns. The final values of the axial component of the alignment tensor in the phage are not significantly different from the initial estimations, as mentioned in the previous section. The convergence of the individual domain structures was similar before and after the combined use of the two types of long-range orientational restraints (Figures 3 and 6). Figure 7 shows that the axes are different between the alignment tensor in the nematic liquid crystalline state of the Pf1 phage and the diffusion tensor in solution, which is probably due to the electrostatic interaction between the Pf1 phage and the Abp1•DNA complex (Zweckstetter and Bax, 2000). Due to this difference in the tensor axes, the combination of the two kinds of orientational restraints was effective for the protein structure calculation of the Abp1•DNA complex.

The overall structure of the two-domain Abp1 protein bound with the DNA

Figure 7 clearly shows that the long axis of the diffusion tensors is oriented between the two recognition helices (third helices in the helix-turn-helix motif).

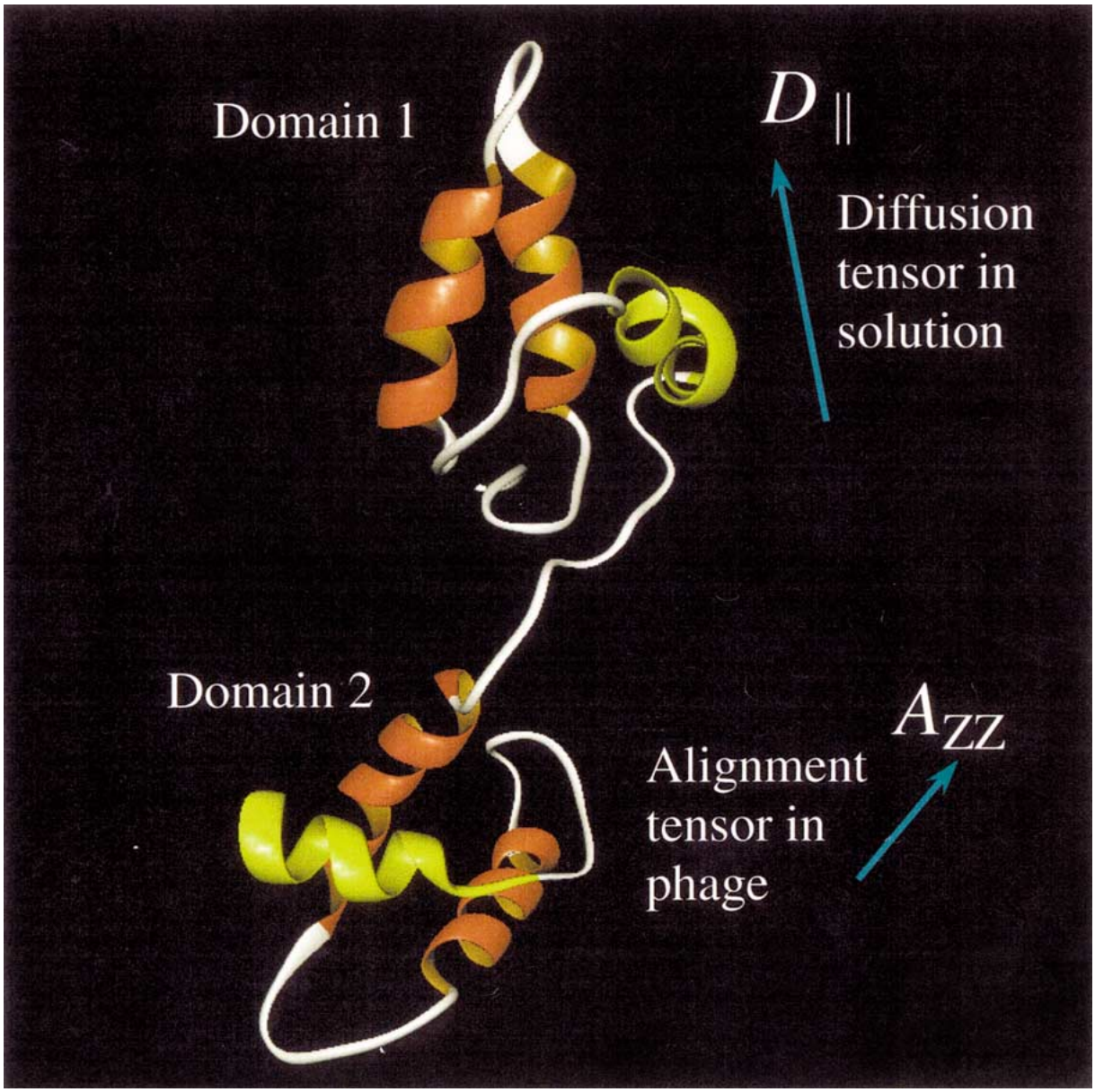

Figure 7. Effect of introducing two different orientational tensors (the NH residual dipolar couplings measured in the Pf1 phage system and the NH rotational diffusion anisotropies measured in solution) in the Abp1 structure calculation. The relative positions of the diffusion tensor in solution and the alignment tensor in nematic phage are indicated with the lowest energy structure of Abp1 in the final structure calculation. This figure was drawn with our in-house program (Sakai et al., manuscript in preparation).

The present structure of the Abp1 protein may fit a 21-bp DNA fragment, as modeled in Figure 8: both of the third helices of the helix-turn-helix motifs could be located in positions suitable for the recognition of the 21-bp DNA fragment. In addition, the DNA helical axis could be oriented in a similar direction to the long axis of the diffusion tensor (Figure 8). Therefore, the relationship between the diffusion tensors of the individual domains, determined by the rotational diffusion data can suggest the overall molecular shape of the complex state. The hydrodynamic calculation based on this complex model (Figure 8) gave 13.1 ns and 2.0 for the overall correlation time, τ_c, and the axial factor of the diffusion tensor, $D_{||}/D_{\perp}$, respectively. These calculated values are similar to the experimental

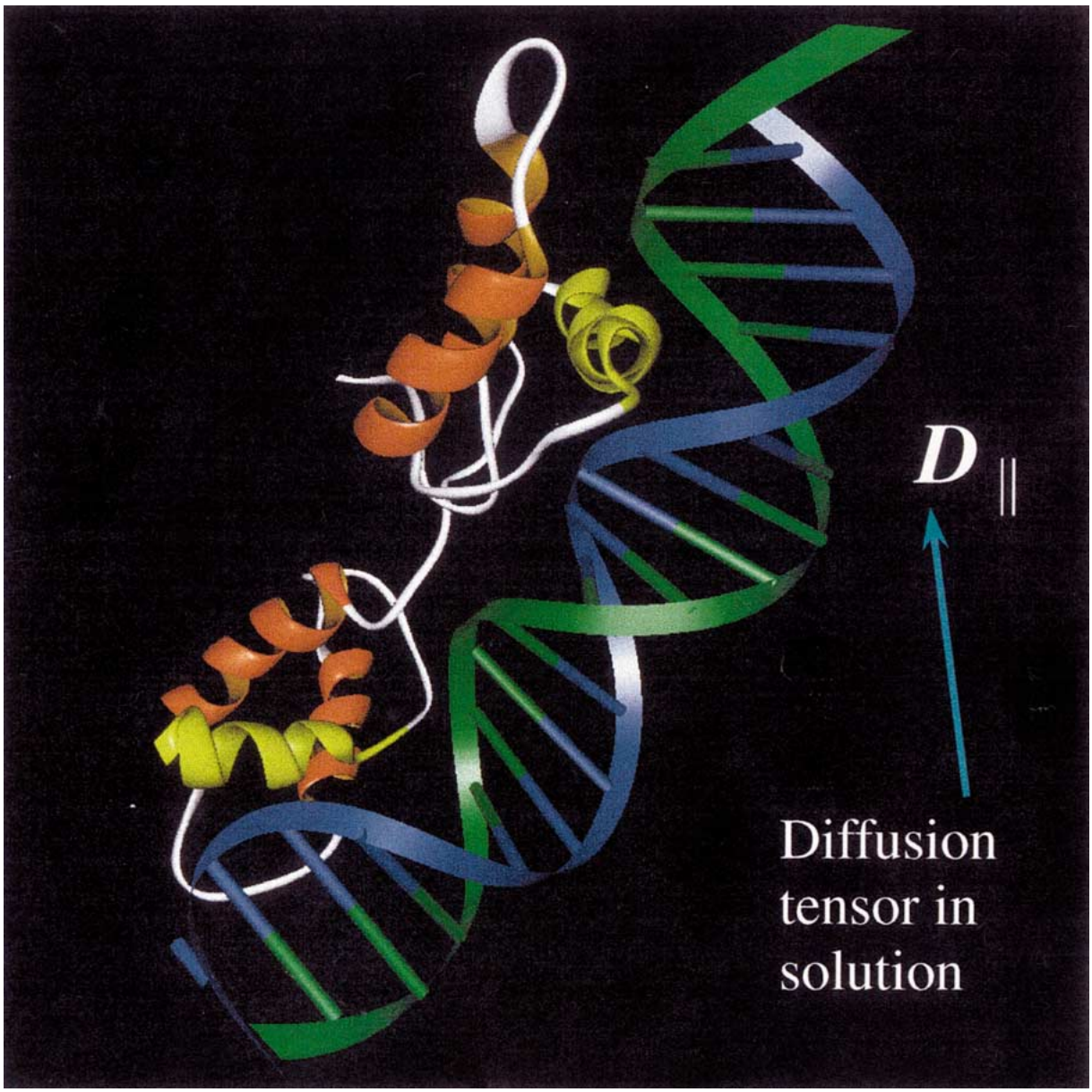

Figure 8. A preliminary docking model of the Abp1•DNA complex.

values (14.2 ns and 2.1, respectively) obtained from the ^{15}N T_1/T_2 ratios.

Acknowledgements

This work was supported in part by a grant from the Biodesign Research Program from RIKEN. J.K. is the recipient of a grant from J.S.P.S.. We thank Yutaka Ito, Makoto Inoue, and Seizo Koshiba for useful discussion, Toshio Yamazaki, Cristina Addy and Michael Williamson for reading of this manuscript, and Saburo Sakai for the use of the in-house graphics program prior to publication.

References

Anderson, N.H., Neidigh, J.W., Harris, S.M., Lee, G.M., Liu, Z. and Tong, H. (1997) *J. Am. Chem. Soc.*, **119**, 8547–8561.

Barbato, G., Ikura, M., Kay, L.E., Pastor, R.W. and Bax, A. (1992) *Biochemistry*, **31**, 5269–5278.

Bax, A. and Grzesiek, S. (1993) *Acc. Chem. Res*., **26**, 131–138.
Brünger, A.T., Adams, P.D., Clore, G.M., DeLano, W.L., Gros, P., Grosse-Kunsteleve, R.W., Jiang, J., Kuszewski, J., Nilges, M., Pannu, N.S., Read, R.J., Rice, L.M., Simnonson, T. and Warren, G.L. (1998) *Acta Crystallogr. Ser. D*, 901–921.
Brüshweiler, R., Liao, X. and Wright, P.E. (1995) *Science*, **268**, 886–889.
Campos-Olivas, R., Newman, J.L. and Summers, M.F. (2000) *J. Mol. Biol*., **296**, 633–649.
Clore, G.M., Gronenborn, A.M and Bax, A. (1998a) *J. Magn. Reson*., **133**, 216–221.
Clore, G.M., Gronenborn, A.M., Szabo, A. and Tjandra, N. (1998b) *J. Am Chem. Soc*., **120**, 4889–4890.
Cornilescu, G., Delaglio, F. and Bax, A. (1998) *J. Biomol. NMR,* **13**, 289–302.
Dosset, P, Hus, J-D., Marion D. and Blackledge, M. (2000) *J. Biomol. NMR*, **16**, 23–28.
Fischer, M.W.F., Losconzi, J.A., Weaver, J.L. and Prestegard, J. (1999) *Biochemistry*, **38**, 9013–9022.
Fushman, D., Weisman, R., Thuring, H. and Ruterjans, H. (1994) *J. Biomol. NMR*, **4**, 61–78.
Fushman, D., Xu, R. and Cowburn, D. (1999) *Biochemistry*, **38**, 10225–10230.
Gardner, K.H. and Kay, L.E. (1998) *Annu. Rev. Biophys. Biomol. Struct*., **27**, 357–406.
García de la Torre, J., Huertas, M.L. and Carrasco, B. (2000) *J. Magn. Reson*., **147**, 138–146.
Garrett, D.S., Seok, Y-J., Liao, D.-I., Peterkofsky, A., Gronenborn, A.M. and Clore, G.M. (1997) *Biochemistry*, **36**, 2517–2530.
Goto, N.K., Skyrynnikov, N.R., Dahlquist, F.W. and Kay, L.E. (2001) *J. Mol. Biol*., **308**, 745–764.
Grzesiek, S. and Bax, A. (1993) *J. Am. Chem. Soc*., **115**, 12593–12594.
Hansen, M.R., Mueller, L. and Pardi, A. (1998) *Nat. Struct. Biol*., **5**, 1065–1074.
Hashimoto, Y., Smith, S.P., Pickford, A.R., Bocquier, A.A., Campbell, I.D. and Werner, J. (2000) *J. Biomol. NMR*, **17**, 203–214.
Kay, L.E., Torchia, D.A. and Bax, A. (1989) *Biochemistry*, **28**, 8972–8979.
King, H.C., Wang, K.Y., Golier, I. and Bolton, P.H. (1995) *J. Magn. Reson.*, **B109**, 323–325.
Mandel, A.M., Akke, M. and Palmer, III, A.G. (1995) *J. Mol. Biol*., **246**, 144–163.
Markus, M.A., Gerstner, R.B., Draper, D.E. and Torchia, D.A. (1999) *J. Mol. Biol.*, **292**, 375–387.
Murakami, Y., Huberman, J.A. and Hurwitz, J. (1996) *Proc. Natl. Acad. Sci. USA*, **93**, 502–507.
Nilges, M., Gronenborn, A.M., Brünger, A.T. and Clore, G.M. (1988) *Protein Eng.*, **2**, 27–38.
Ottiger, M. Delaglio, F. and Bax, A. (1998) *J. Magn. Reson.*, **131**, 173–178.
Ramirez, B.E. and Bax, A. (1998) *J. Am. Chem. Soc*., **120**, 9106–9107.
Smith, S.P., Hashimoto, Y., Pickford, A.R., Campbell, I.D. and Werner, J.M. (2000) *Biochemistry*, **39**, 8374.
Stein, E.G., Rice, L.M. and Brünger, A.T. (1997) *J. Magn. Reson.*, **124**, 154–164.
Tjandra, N. and Bax, A. (1997) *Science*, **278**, 1111–1114.
Tjandra, N., Feller, S.E., Pastor, R.W. and Bax, A. (1995) *J. Am. Chem. Soc.*, **117**, 12562–12566.
Tjandra, N., Garrett, D.S., Gronenborn, A.M, Bax, A. and Clore, G.M. (1997a) *Nat. Struct. Biol.*, **4**, 443–449.
Tjandra, N., Omichinski, J.D., Gronenborn, A.M., Clore, G.M. and Bax, A. (1997b) *Nat. Struct. Biol*., **4**, 732–738.
Tjandra, N., Szabo, A. and Bax, A. (1996) *J. Am. Chem. Soc.*, **118**, 6986–6991.
Tolman, J.R., Flanagan, J.M., Kennedy, M.A and Prestegard, J.H. (1995) *Proc. Natl. Acad. Sci. USA*, **92**, 9279–9283.
Tsan, P., Hus, J.-C., Caffrey, M., Marion, D. and Blackledge, M. (2000) *J. Am. Chem. Soc.*, **122**, 5603–5612.
Tsui, V., Zhu, L., Huang, T.H., Wright, P.E. and Case, D.A. (2000) *J. Biomol. NMR*, **16**, 9–21.
Yoshida, T., Uchiyama, S., Nakano, H., Kashimori, H., Kijima, H., Ohshima, T., Saihara, Y., Ishino, T., Shimahara, H., Yoshida, T., Yokose, K., Ohkubo, T., Kaji, A. and Kobayashi, Y. (2001) *Biochemistry*, **40**, 2387–2396.
Woessner, D.E. (1962) *J. Chem. Phys*., **36**, 1–4.
Zweckstetter, M. and Bax, A. (2000) *J. Am. Chem. Soc*., **122**, 3791–3792.